Applied Catalysis B: Environmental 275 (2020) 119119

Contents lists available at ScienceDirect

Applied Catalysis B: Environmental

journal homepage: www.elsevier.com/locate/apcatb

First discernments for NO storage and reduction (NSR) on lithium cuprate (Li_2CuO_2) at moderate temperatures ($100 \leq T \leq 400\,^{\circ}C$)

Ana Yañez-Aulestia, Heriberto Pfeiffer*

Laboratorio de Fisicoquímica y Reactividad de Superficies (LaFReS), Instituto de Investigaciones en Materiales, Universidad Nacional Autónoma de México, Circuito exterior s/n, Cd. Universitaria, Del. Coyoacán C.P. 04510, Ciudad de México, Mexico

ARTICLE INFO

Keywords:
Lithium cuprate
NO sorption
NO storage and reduction (NSR)

ABSTRACT

The present study was carried out to analyze the NO storage and reduction (NSR) on Li_2CuO_2. The objective of this investigation was to determine the first insights of NSR, while using a new material. Li_2CuO_2 was initially evaluated as NO sorbent (2 mL/min) in the presence of different oxygen contents. These results were used to verify the NO consumption and chemical sorption and to propose a reaction mechanism for the lithium nitrate formation. The best NSR results were obtained between 200 and 300 °C and Li_2CuO_2 showed high stability during cycling processes. A reaction mechanism, based on the Mars–Van Krevelen model was presented. After that, similar experiments were performed but using a lower NO concentration (777 ppm), where the results were equivalent to those obtained with higher NO concentrations. Thus, results establish interesting bases to analyze and allow to a double NO NSR-SCR process in the future, using alkaline ceramics.

1. Introduction

In the last two decades, one of the most threatening global problems is related to different energetic and environmental issues [1]. Within this big issue, the pollution produced by nitrogen oxides (NO, NO_2 and N_2O), chemically generalized as NO_x, contribute to a series of environmental problems, although they are not the polluted gases with the highest concentrations on the atmosphere [2–4]. Nitrogen oxides are produced on stationary industrial installations, such as coal-consuming power plants and industrial boilers, among others [5], and they are responsible for the photochemical smog and the acid rain [6]. Based on that, the scientific community has established different approaches for the NO_x elimination: *i*) the NO_x storage and reduction (NSR), which implies the NO_x oxidation and separation as nitrites or nitrates and *ii*) NO_x selective catalytic reduction (SCR), implying a simultaneous sorption and catalytic reaction with other species such as carbon monoxide (CO) or ammonia (NH_3) [7–12].

For the NSR process, NO is oxidized to NO_2^{1-} or NO_3^{1-} species, producing nitrites or nitrates, respectively. This reaction mechanism is mostly performed over noble metals in presence of a basic compound [13–15]. In general, the materials used for this application have the following chemical content; nobel metal/BaO/ceramic support, where the nobel metal is usually platinum, while the ceramic supports are alumina (Al_2O_3) or ceria (CeO_2) [13,16–20]. About the basic compound, most of the reports published on literature used barium or strontium oxides, and only a few other reports used some perovskites with lower basic properties [21–25]. Therefore, the development and analysis of different materials, as possible variants for the nobel metal and barium oxide materials would be of great interest from several points of view.

Recently, the application of copper-containing materials, not for the NSR process, but for the carbon monoxide selective catalytic reduction (CO-SCR) of NO has been reported [26–28]. These materials have received extensive attention, as in several cases, the presence of novel metals are not needed. For example, it has been demonstrated that CuO particles deposited on titania (TiO_2) supports have excellent activity in the CO-SCR reaction [29]. More recently, as another example, it was reported that copper nanoparticles deposed over carbon supports are able to perform the NH_3-SCR reaction process at moderate temperatures [27]. Thus, copper-containing materials seem to possess good properties for the NO selective catalytic reduction process.

On the other hand, lithium cuprate (Li_2CuO_2) is a highly alkaline ceramic, which has been proposed for different applications such as lithium-ion batteries [30–32] and as CO_2 and CO captor material [33–35]. Li_2CuO_2 has a laminar structure formed by [CuO_4] plane squares and lithium cations located into the interlayer spaces [36,37]. This crystal structure produces a high lithium cation mobility, which is the main reason for using Li_2CuO_2 in these applications. Moreover, the gas sorption applications have been established based on the same

* Corresponding author.
E-mail address: pfeiffer@materiales.unam.mx (H. Pfeiffer).

https://doi.org/10.1016/j.apcatb.2020.119119
Received 9 April 2020; Received in revised form 7 May 2020; Accepted 9 May 2020
Available online 17 May 2020
0926-3373/

lithium cation mobility, but as well on the basic particle surface and redox cupper properties [33,35]. Based on all the previous descriptions, the aim of this work was to analyze the NO possible consumption and sorption on Li_2CuO_2, in the presence of different amounts of oxygen. This work is presented as a first insight of the possible utilization of this lithium ceramic within the NO_x reduction process, either under the NSR and/or SCR schemes.

2. Experimental section

Li_2CuO_2 sample was obtained by solid-state reaction where the precursors, lithium oxide (Li_2O, Aldrich) and copper oxide (CuO, Meyer), were mechanically mixed and heated at 800 °C for 6 h in air [38]. It was characterized by X-ray diffraction (XRD) and fitted with 01-073-2324 JCPDS file, which corresponded with the Li_2CuO_2 orthorhombic crystalline phase. Moreover, the N_2 adsorption-desorption isotherm of the sample was obtained to determine the BET specific surface area of the sample; 2.0 m^2/g (data not shown). Finally, the pristine Li_2CuO_2 was characterized by X-ray photoelectron spectroscopy (XPS), using a KAlpha Thermo Scientific spectroscopy equipment. It provided an X-ray source and Al-K_α monochromatic radiation. An argon beam was used to eliminate sample surface impurities. Moreover, the C_{1s} peak (284.6 eV) was used for energy calibration.

Different gas sorption experiments were performed using a catalytic flow reactor (CATLAB-PCS, Hiden Analytical) coupled with QGA mass spectrometer (Hiden Analytical), using the following MS numbers for the NO, N_2O and NO_2 identification, 30, 44 and 46 amu, respectively. All these experiments were carried out using NO (Praxair, 2% N_2 balanced), O_2 (Praxair, grade 2.6) and N_2 (Praxair, grade 4.8). N_2 was used as a gas balance and as the carrier gas, using in all the experiments a total flow rate of 100 mL/min. Dynamic and isothermal profiles were obtained using 0.1 g of Li_2CuO_2 in each experiment. For an initial set of experiments, dynamic experiments were performed from 30 to 500 °C, using different NO:O_2 ratios (1:4, 1:2 and 1:1). Then, the isothermal analyses were carried out at different temperatures, between 100 and 450 °C. In the isothermal experiments, samples were heated to the desired temperature under a N_2 flow (60 mL/min), and once each sample reached the corresponding temperature, the gas flow was switched to the corresponding gas mixture, with a total flow of 100 mL/min. The isothermal condition was kept during eight hours. After that, cyclic experiments (10 cycles) were performed at 300 °C, using the three different NO:O_2 ratios during sorption (1 h) and N_2-O_2 (P_{O2}:P_{N2} = 0.05:0.95) for desorption process at 650 °C during 1 h. The isothermal and cyclic Li_2CuO_2 products were analyzed by XRD, ATR-FTIR and TG. The XRD patterns were obtained with a D5000 Siemens diffractometer coupled to a Co anode X-ray tube. Compounds were identified using the Joint Committee Powder Diffraction Standards (JCPDS) database. The ATR-FTIR spectra ($4000-400\ cm^{-1}$) were obtained using ALPHA-Platinum equipment from Bruker. Finally, the thermogravimetric analyses were performed from 40 to 850 °C in a thermogravimetric balance Q500HR, from TA Instruments in order to determine the presence of different species on the samples.

Based on the previous experiments, new experiments were performed at a lower NO concentration (777 ppm), simulating a real NO concentration. In this case, dynamic experiments were performed from 30 to 320 °C, varying the O_2 contents (4, 6, 8, 10 mL/min). The isothermal experiments were obtained between 100 and 300 °C, only using 4 mL/min of oxygen for 180 min. Two different cyclic experiments were performed at 300 °C using 777 ppm of NO and 4 mL of oxygen in the sorption process, while the previously described N_2-O_2 gas mixture was used at 650 °C during the desorption process. The first cyclic experiment had 10 cycles, 1 h of sorption and 1 h of desorption. Conversely, the second cyclic experiment consisted of 5 cycles, which were performed during 8 h of sorption and 1 h of desorption. As in the first set of experiments, isothermal and cyclic sample products were analyzed by XRD.

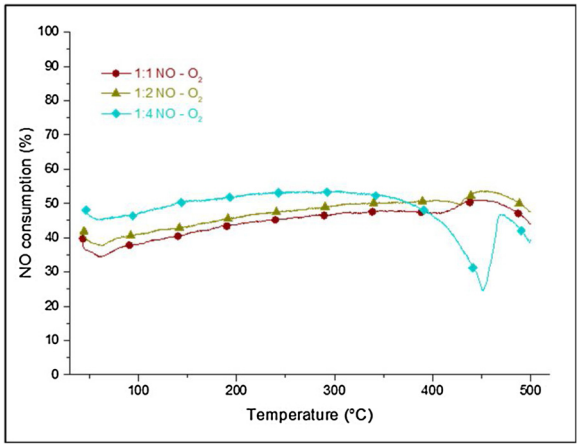

Fig. 1. Dynamic evolution of the NO consumption as a function of temperature, varying the oxygen concentration.

3. Results and discussion

As it was mentioned on the introduction section, Li_2CuO_2 presents great basic chemical properties, probed by the CO and CO_2 sorption capacities, two acid molecules [33]. Based on that, and the fact that NO is another acid gas, its sorption possibility, on Li_2CuO_2, was analyzed. Thus, different dynamic experiments, between 30 and 500 °C, were performed varying the NO:O_2 ratio (Fig. 1). These initial experiments were performed using a NO concentration of 2 %, N_2 balanced (see experimental section) in the presence of different amounts of oxygen. All the NO:O_2 ratios presented similar NO consumption trends between 30 and 320 °C, getting the best NO consumptions (around 50 %) when the NO:O_2 ratio was 1:4. Nevertheless, at higher temperatures ($T \leq 380$ °C), this NO:O_2 ratio importantly decreases the NO consumption, something almost not presented when lower O_2 amounts were used. This result is produced by different factors: The amounts of NO sorbed saturated and blocked the Li_2CuO_2 particle surface inhibiting further sorptions, but mainly due to the oxygen adsorption produced during the nitrate formation, which competes by the adsorption sites, as it is described below. Moreover, $LiNO_3$ decomposes at this temperature range. So, the NO sorption-desorption equilibrium must be affected at $T > 450$ °C. It must be mentioned that during these experiments all the other possible NO_x gases were followed by the mass spectrometer, not observing any of them (data not shown).

Based on the dynamic results, all the NO:O_2 ratios were isothermally tested, to further analyze the process. Fig. 2 shows the results obtained when the NO:O_2 ratio was 1:4, in order to deeply visualize, analyze and understand the NO sorption and consumption evolution processes on Li_2CuO_2. The isotherm performed at 100 °C presented a continuous NO consumption of ~49 %, being highly stable during the whole isothermal process (480 min). Then, the isotherm performed at 200 °C presented similar stability, although the NO consumption was importantly higher, 70 %. In fact, at this thermal condition, the NO consumption presented its highest value. Isotherms performed between 250 and 350 °C decreased the NO consumption between 65 and 50 %. Then, the NO consumption decrement continued as a function of temperature, as the isotherms obtained at 400 and 450 °C presented the lowest values. The differences observed between the isotherms and the dynamic experiments (see Fig. 1) can be explained by the different equilibrium regimes present in each experimental set; non-equilibrium and equilibrium systems are presented during the dynamic and isothermal experiments respectively.

All the isothermal Li_2CuO_2 products were analyzed by XRD and ATR-FTIR. These results are presented in Fig. 3. The XRD patterns presented an evolution of the crystalline phases as a function of temperature (Fig. 3-A). Between 100 and 250 °C, it is clearly evident that

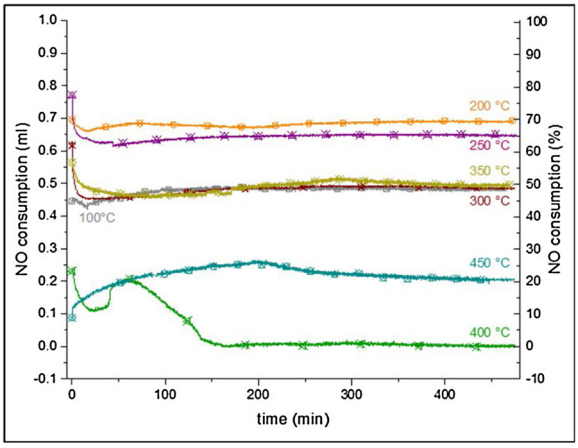

Fig. 2. Dynamic evolution of NO obtained during the isothermal processes performed on Li_2CuO_2 at different temperatures. The NO:O ratio used for these isotherms was 1:4.

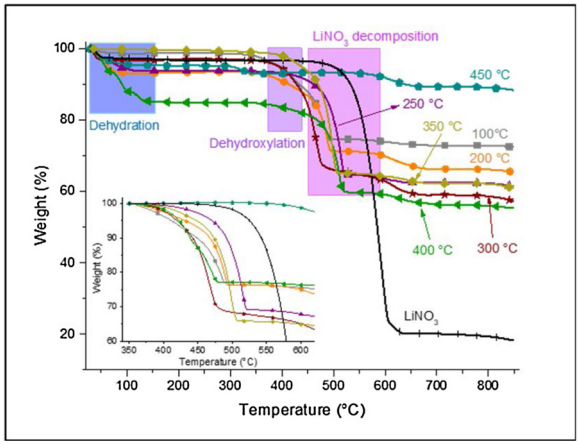

Fig. 4. Decomposition thermograms of the Li_2CuO_2 isothermal products obtained after the NO:O_2 process, where the NO:O ratio was 1:4. The square inset shows a normalized amplification of the nitrate decomposition temperature range.

Li_2CuO_2 tended to decrease, while CuO (JCPDS file 00-005-0661) increased. In none of these cases was possible to determine any lithium secondary phase, despite the CuO formation. In fact, at 300 °C, the only phase detected in the corresponding diffraction pattern was CuO, indicating that Li_2CuO_2 is being consumed. Then, between 350 and 400 °C it was possible to identified lithium nitrate ($LiNO_3$, JCPDS file 01-080-0203) as a lithium containing crystal phase, confirming the NO chemical sorption on Li_2CuO_2. Finally, at 450 °C Li_2CuO_2 was the unique crystal phase obtained, in good agreement with the low NO consumption observed dynamic and isothermally at this temperature. Something else must be pointed out from these XRD patterns. The CuO diffraction peaks are importantly wide in all the cases, indicating the formation of nanocrystals. Thus, the CuO crystal sizes were determined by using the Scherrer equation [39]. The corresponding measurements indicated that CuO crystals grew from 240 to 453 Å, while increasing the isothermal temperature from 100 to 400 °C. Thus, the formation of CuO nanocrystals must be related to the Li_2CuO_2 partial and continuous degradation produced by the NO chemical sorption, while CuO crystal growth must simply be attributed to the temperature in which each isothermal experiment was performed.

The NO chemical sorption was corroborated by ATR-FTIR (Fig. 3-B). The characteristic vibrations of the N–O bond were identified on the Li_2CuO_2 isothermal products obtained between 200 and 400 °C. An anti-symmetrical vibration mode of stretching is located at 1380 cm^{-1}, and this energy absorption is considered the most intense. Although the symmetric vibration mode is inactive in infrared, there are two modes of angular deformations for O–N–O bonds in infrared at 830 and 720 cm^{-1}. Besides, the bands associated with monodentate nitrates at approximately 1035 cm^{-1} were presented [40,41]. Then, although $LiNO_3$ was not identified on the XRD patterns obtained at T < 300 °C, it was possible to identify it by ATR-FTIR. It may be simply explained based on the $LiNO_3$ dispersion or crystal sizes produced over the Li_2CuO_2 surface particles. Moreover, the ATR-FTIR spectra confirmed that $LiNO_3$ was not formed at 450 °C, as it was shown by the corresponding XRD pattern. It must be mentioned that some other bands were detected, in addition to the nitrate vibration bands. These vibration bands were attributed to CO_3^{2-} (860 cm^{-1}) and OH^{1-} (3600 − 3540 cm^{-1}) species [42]. The presence of these carbonates and hydroxides ions must be simply explained by the carbonation and hydration-hydroxylation produced during the environmental atmospheric manipulation of the Li_2CuO_2 sample products.

To complement the Li_2CuO_2 isothermal product characterization, all of them were analyzed by TG analysis (Fig. 4). All these products presented three different weight loss attributed to dehydration (T ≤ 100 °C), dehydroxylation (between 380 and 440 °C) and denitration (T ≥ 450 °C). The first two processes (dehydration and dehydroxylation) must correspond to water sorbed on the products during the sample air exposition produced after the isothermal processes. In fact, $LiNO_3$ is highly hygroscopic. So, the isothermal sample produced at 400 °C, presenting the largest amount of lithium nitrate, was the sample more hydrated. This TG result is in good agreement with all previous

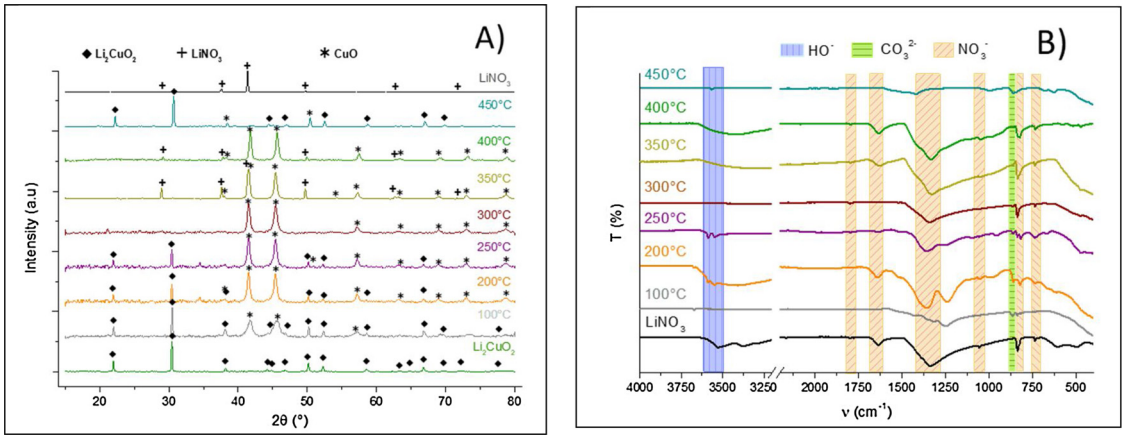

Fig. 3. XRD patterns (A) and ATR-FTIR spectra (B) of the Li_2CuO_2 isothermal products obtained after the NO:O_2 process, where the NO:O ratio was 1:4. The pristine Li_2CuO_2 and $LiNO_3$ patterns and spectra are included for comparison purposes.

results. Then, the denitration process corresponds to the $LiNO_3$ decomposition. In fact, the pristine $LiNO_3$ decomposition was incorporated on this figure, for comparison purposes. The amounts of weight loss attributed to denitration process were between 22 and 34 wt%, although the Li_2CuO_2 sample product obtained at 450 °C practically did not present this weight loss. Again, these results confirm that NO is being chemically trapped on Li_2CuO_2, but the NO chemisorption is only produced between 100 and 400 °C.

All these results confirmed that Li_2CuO_2 is able to trap, chemically, NO between 100 and 400 °C, obtaining the highest NO consumptions at around 200 − 250 °C. The most probable reaction mechanism may be the Mars–van Krevelen reaction mechanism model [43], which is well accepted for oxidation processes involving reducible metal oxides. In fact, this model has been already proposed for the carbon monoxide chemisorption on lithium cuprate and other lithium ceramics [35,44]. In fact, it is well known that lattice oxygen mobility and release are highly important in the Mars–van Krevelen model. Based on that the XPS spectrum of Li_2CuO_2 was obtained to determine its oxygen binding energy (see supplementary Figure S1). The O(1 s) binding energy was measured at 532.0 eV, which is a similar but slightly higher value than those values reported for copper oxides; CuO (529.5 eV) and Cu_2O (530.5 eV) [45]. It means that oxygen binding energy on Li_2CuO_2 should have similar release availability than copper oxides, which have excellent characteristics. Thus, this model implies that NO is adsorbed on the Li_2CuO_2 surface, which releases oxygen anions. Moreover, these anionic vacancies must be immediately occupied and used for the O_2 adsorption and homolytic dissociation, completing the lithium nitrate formation. This general process is presented in reaction 1.

$$Li_2CuO_2 + 2\ NO + 1.5\ O_2 \longrightarrow 2\ LiNO_3 + CuO \quad (1)$$

The assumption that NO is adsorbed with the subsequent oxygen release, from the Li_2CuO_2 crystal structure, is based on the following two facts; *i*) that lithium cuprate was able to consume NO, even in the absence of oxygen (data not shown). In such a case, copper must be reduced to metallic copper, releasing all the oxygen anions from the lithium cuprate crystal structure. *ii*) It has been reported on literature that Li_2CuO_2 has high reducibility properties. It was evidenced through CO-TPR, TG and catalytic experiments [33,35]. In those cases, it was shown that Cu^{2+}, initially contained on the Li_2CuO_2 crystal structure, can be easily reduced to Cu^{1+} or Cu^0, due to oxygen release. Thus, the whole NO reaction evolution performed on Li_2CuO_2, through the Mar − Van Krevelen mechanism, is summarized in reactions 2 to 4:

$$NO \xrightarrow{Li_2CuO_2} NO_2^{1-} + Li_{Li} + Cu_{Cu}^{\cdot\cdot} + V_o^{\cdot\cdot} \quad (2)$$

$$V_o^{\cdot\cdot} + O_{2(g)} \rightarrow 2O^{\bullet} \quad (3)$$

$$NO_2^{1-} + O^{\bullet} \rightarrow NO_3^{1-} \quad (4)$$

In order to analyze the reproducibility of NO sorption and Li_2CuO_2 stability, different cyclic experiments were performed analyzing the gas evolution during cycles as well as the sample composition at the end of the whole process. Fig. 5-A shows the evolution of NO, other possible NO_x and O_2 gases as a function of temperature, during the first cycle. In the first hour, at 300 °C, the determined amounts of NO (O_{NO}) and O_2 (O_{O2}) consumed were relatively constants, showing good consumption stability of the process. They were based on the few NO (F_{NO}) and O_2 (F_{O2}) amounts. Then, as soon as the NO flow was closed and temperature began to increase, there was a sudden but important O_2 consumption, suggesting high oxygen sorption on the Li_2CuO_2 sample, with the subsequent oxygen stabilization. This high oxygen consumption indicates the deficiency of this element on the Li_2CuO_2 sample product after the NO flow, which must be produced due to the NO oxidation to nitrates, as explained above. After that, during the heating process (between 450 and 540 °C), the sample evidenced the NO and O_2 desorptions. This result shows that reaction 1 is reversible at high

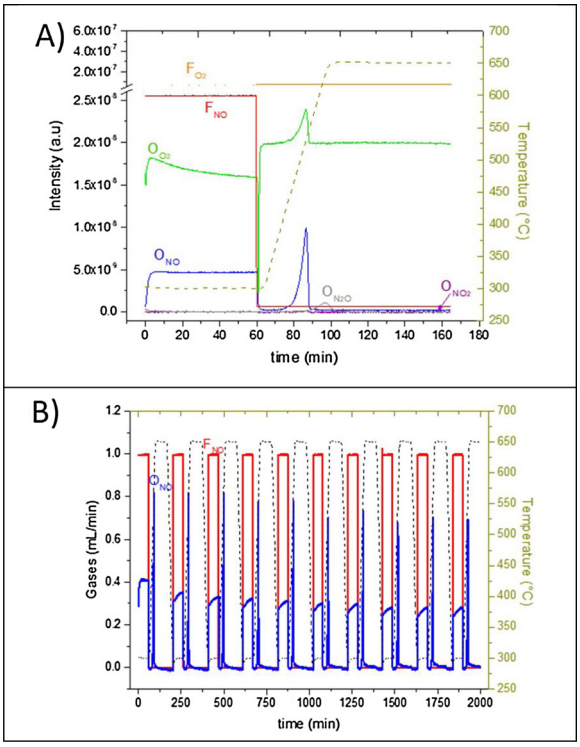

Fig. 5. Dynamic evolution of gases produced during the sorption and desorption cyclic experiment. The first cycle (A) presents NO and O_2 volume feeds (F_{NO} and F_{O2}) as well as the corresponding concentrations at the sweep (O_{NO} and O_{O2}). Moreover, the N_2O and NO_2 production were followed. Ten cycles curve (B) only shows the NO evolutions.

temperatures in the oxygen presence, of course. Finally, it must be mentioned that N_2O desorption was observed between 550 and 650 °C, while NO_2 was never detected, unless it had rapidly evolved to NO. In such a case, it would be involuted as part of the NO signal. The presence of small amounts of N_2O, after most of the NO desorption, indicates that residual amounts of lithium nitrate decompose as it is shown in reaction 5, where the produced Li_2O must react with CuO regenerating Li_2CuO_2, during the same heating process. After the analysis of the first cycle, ten new cycles were performed consecutively (Fig. 5-B). The Li_2CuO_2 sample presented good stability during all these cycles, as the amounts of NO consumed and desorbed only presented a slight decrement after 10 cycles.

$$2\ LiNO_3 \rightarrow N_2O + Li_2O + 2\ O_2 \quad (5)$$

The cyclic experiment was repeated varying the oxygen content, where the results showed two different trends. In one hand, independently of the NO:O_2 ratio the NO consumption increased as a function of the cycles. It must be attributed to the Li_2CuO_2 microstructural evolution produced on these materials after the gas chemical sorption and crystal regeneration [46]. On the other hand, it can be seen that high NO sorption-desorption stabilities for all the NO:O_2 ratios, where the oxygen concentration slightly increases the cyclic efficiency (Fig. 6-A). After the different cyclic experiments, all the Li_2CuO_2 products, after a final NO desorption step, were re-analyzed by XRD and compared with the pristine Li_2CuO_2 and $LiNO_3$ samples (Fig. 6-B). Independently of the oxygen content, all the Li_2CuO_2 cyclic products were composed of Li_2CuO_2 and CuO. This result shows that part of the Li_2CuO_2 is been decomposed through the cycles. The Li_2CuO_2 partial decomposition must be produced during the heating NO desorption process, where lithium may have sublimed. This assumption is supported by the N_2O desorption, which implies the Li_2O production (see reaction 2), which must be mostly reincorporated into the Li_2CuO_2

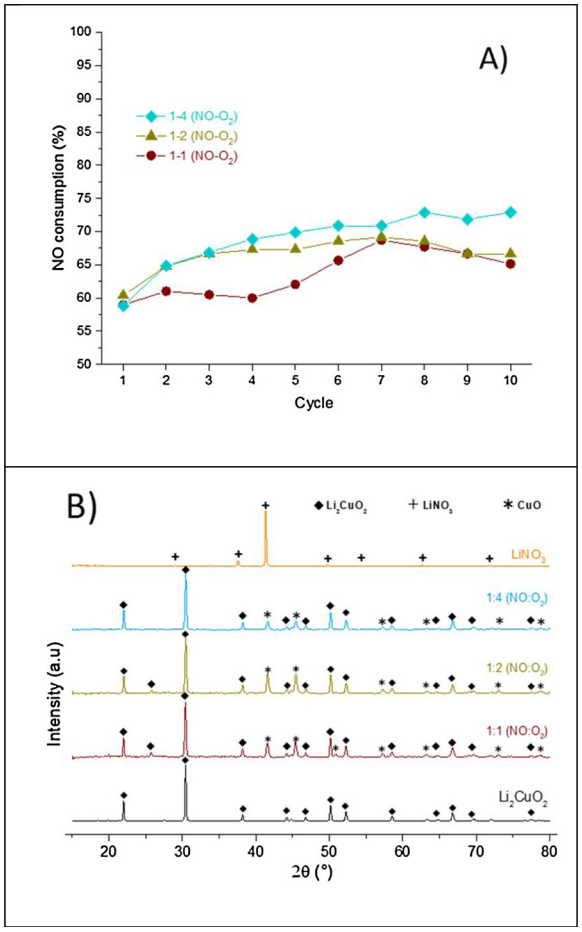

Fig. 6. NO consumption efficiencies (A) and XRD patterns of the Li_2CuO_2 cyclic products (B) obtained using different NO:O_2 ratios. The pristine Li_2CuO_2 and $LiNO_3$ patterns are included for comparison purposes.

crystal structure, but part of it must have sublimed as well, as it is well known [35].

After the whole analysis performed on Li_2CuO_2 for the NO sorption, using a high NO concentration, the same analysis was performed, but using a much lower NO concentration (777 ppm), which is a close concentration than that presented in real gas polluted systems. Then, as in the previous cases showed above, dynamic experiments were initially performed varying the O_2 content (Fig. 7). All these systems presented

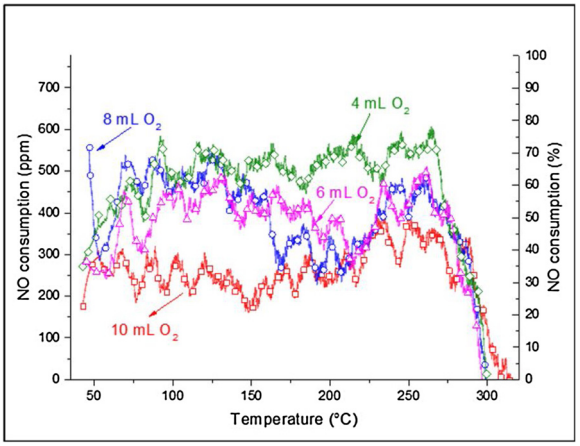

Fig. 7. Dynamic evolution of the NO consumption as a function of temperature, using a low NO concentration (777 ppm) and varying the oxygen contents.

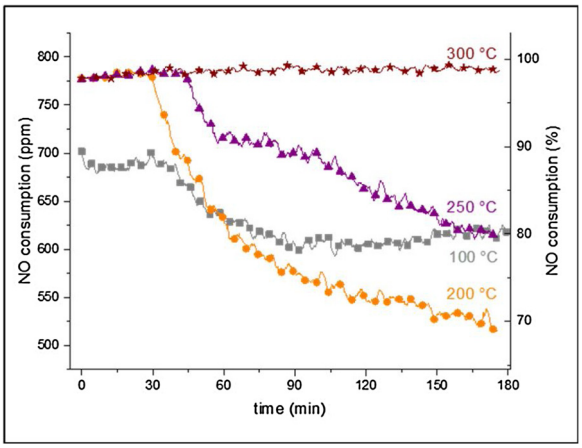

Fig. 8. Dynamic evolution of NO (777 ppm) obtained during the isothermal process performed on Li_2CuO_2 at different temperatures, using 4 mL/min.

important NO consumptions, depending on the oxygen content, where the best NO consumptions (around 70 %) were observed with an O_2 flow content of 4 mL/min. It must be noticed that the NO consumption tended to decreased when the O_2 contents increased. It seems that high oxygen concentration inhibits the NO consumption, probably as there may be an adsorption sites competition between the two gases. Furthermore, the NO consumption tended to decrease at temperatures higher than 275 °C, independently of the oxygen content. This is a similar behavior than that observed with a larger NO concentration. Nevertheless, in this case, the NO consumption decrement was observed at a lower temperature. This thermal shift can be explained based on the NO sorption-desorption equilibrium, which was shifted to a lower temperature due to the low NO concentration.

Based on the NO sorption dynamic results, different isothermal experiments were performed between 100 and 300 °C using 4 mL/min of oxygen (Fig. 8). At 100 °C, the isothermal trend decreased from 90 to 80 % of efficiency through the 180 min. Then, at higher temperatures, the initial NO consumption was total (100 %), at least during the first minutes. However, isotherms performed at 200 and 250 °C only showed a total NO consumption during the initial 30 – 40 min, decreasing to 70 and 80 % of efficiency after 3 h, respectively. Conversely, the isothermal experiment performed at 300 °C presented a 100 % of efficiency during all the experimental time. Here, the high NO consumption should be attributed to its low concentration, in comparison to the NO high concentration results observed above, where the $LiNO_3$ production must have saturated the Li_2CuO_2 surface. In these cases, the XRD and ART-FTIR results did not evidence clearly the presence of $LiNO_3$ (see supplementary Figure S2), although the presence of CuO confirmed that Li_2CuO_2 did partially reacted with NO. Thus, the $LiNO_3$ must be highly dispersed ad out of the detection limit of this technique. Complementarily, the ATR-FTIR spectra of these isothermal products slightly depicted the corresponding nitrate vibration bands. However, another isothermal experiment was performed at 300 °C during 12 h, where a whole efficiency (100 %) was maintained. Moreover, the XRD pattern and ATR-FTIR spectrum of that isothermal Li_2CuO_2 product did show the formation of $LiNO_3$ (see supplementary Figure S3).

Based on the fact that Li_2CuO_2 was able to trap NO isothermally, even at low concentrations, two different sets of cyclic experiments were performed, where the NO consumption times were varied. In the first case, identical NO sorption-desorption conditions were used, in comparison to those conditions used with the high NO concentration. Fig. 9 shows that NO and O_2 presented the same trends than those described above, using a high NO concentration. Of course, the amounts of NO consumed were slightly higher in this case, because the ceramic is able to trap more NO during longer times, due to the lower concentration. However, the efficiency of NO consumption varied when

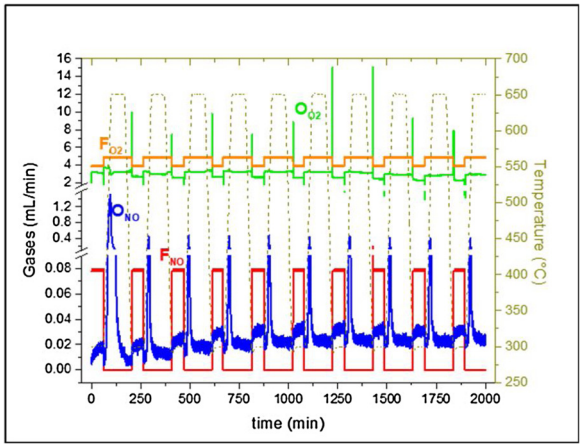

Fig. 9. Dynamic evolution of NO and O_2 produced during the sorption (1 h) and desorption (1 h) cyclic experiment, using a low NO concentration (777 ppm). NO and O_2 volume feeds (F_{NO} and F_{O2}) as well as the corresponding concentrations at the sweep (O_{NO} and O_{O2}) are presented.

the NO concentration was reduced, moving 65–70 % to 80–85 %, while the NO concentration decreased. It may be explained base on the fact of an adsorption sites unsaturation, allowing to higher efficiencies.

Something important must be taken into account for the cyclic experiments. In the NO low concentration case, the possible amount of $LiNO_3$ produced during the sorption step is importantly low. Thus, longer NO sorption time may be expected and performed. Based on that, a second cyclic experiment was performed, but in this case, the NO consumption time was 8 h (Fig. 10). The general trend was similar to previous cases. Nevertheless, the NO sorption time allowed to evidence how the amounts of NO at the exit (O_{NO}) increased as a function of time, from almost zero to $0.02 - 0.025$ mL/min (Fig. 10-A). This change must be attributed to a partial NO sorption saturation presented by the Li_2CuO_2 sample through the time. Then, when the two sets of cyclic experiments are compared different issues must be pointed out (Fig. 10-B). First, when the NO consumption is compared as a function of the cycle number, the experiments showed NO consumptions between 85 and 76 %, where the short time cycles apparent better consumptions. Nevertheless, it must be taken into account that one long time NO consumption cycle is sorbing much longer amounts of NO. These larger NO amounts, which must be associated to $LiNO_3$ and CuO formation, should slightly decrease the average NO consumption during one cycle process. Thus, when the cycles are compared as a function of time (square inset of Fig. 10-B), it is more evident that long NO consumption cycle processes converting more NO amounts, even though this experiment only was performed during five cycles.

Finally, after both cyclic experiments, the Li_2CuO_2 sample products were analyzed by XRD, and compared, again, with pristine Li_2CuO_2 and $LiNO_3$ (Fig. 11). As it would be expected, the Li_2CuO_2 cyclic products obtained after the larger NO sorption steps evidenced a higher lithium cuprate partial decomposition, as the amounts of CuO were more evident. This result suggests a larger Li_2O sublimation produced during the $LiNO_3$ decomposition, as explained above.

4. Conclusions

In the present work, the NO storage and reduction on Li_2CuO_2 was analyzed, using different physicochemical conditions. First, and in order to determine the NO reactivity with Li_2CuO_2, a relatively large NO concentration was used, 2 mL/min in the presence of different amounts of oxygen (N_2 balanced to total flows of 100 mL/min). Different dynamic and isothermal experiments were performed, where relatively high NO consumption efficiencies were observed, without the formation of any other NO_x specie. The NO consumption was confirmed

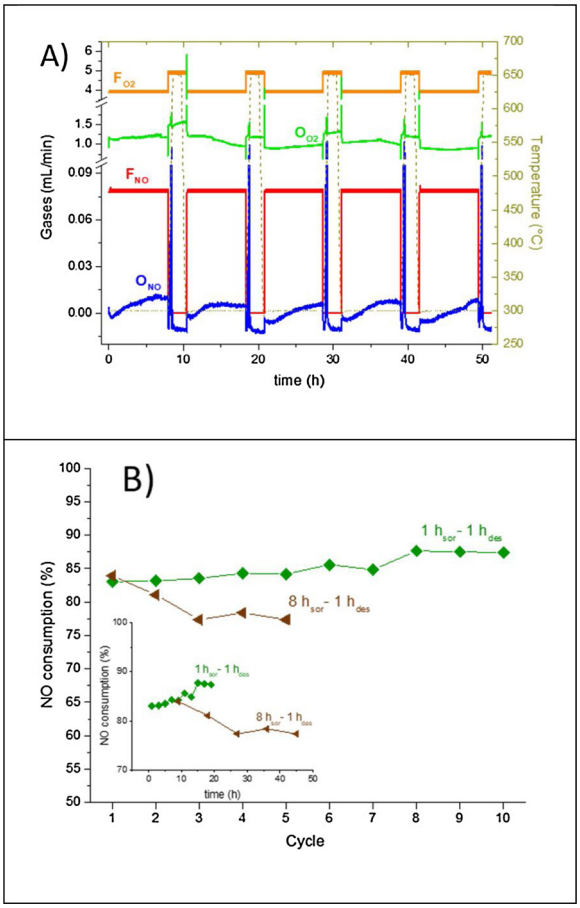

Fig. 10. Dynamic evolution of NO and O_2 produced during the sorption (8 h) and desorption (1 h) cyclic experiment (A), using a low NO concentration (777 ppm). NO and O_2 volume feeds (F_{NO} and F_{O2}) as well as the corresponding concentrations at the sweep (O_{NO} and O_{O2}) are presented. NO consumption comparison as a function of the cycles and sorption time (B).

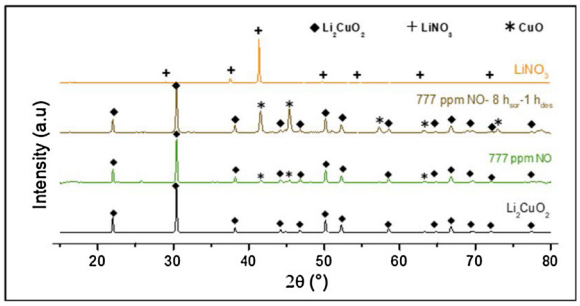

Fig. 11. XRD patterns of the different Li_2CuO_2 cyclic products using a low NO concentration (777 ppm), where the pristine Li_2CuO_2 and $LiNO_3$ patterns are included for comparison purposes.

by the Li_2CuO_2 isothermal products analyses, which were performed by XRD, ATR-FTIR and TG analyses. All these techniques evidenced the formation of $LiNO_3$ and CuO produced due to the NO chemical capture process performed on Li_2CuO_2. All these experimental data allowed to determining and proposing a reaction mechanism, based on the Mars–van Krevelen reaction model, well accepted for oxidation processes involving reducible metal oxides. After that, a cyclic experiment was performed to determine the Li_2CuO_2 stability. Results evidence a high NO chemical sorption during ten cycles, and it was observed that during $LiNO_3$ decomposition, NO is mainly produced although small amounts of NO_2 were detected.

After evidencing the NO consumption and chemical reaction with Li_2CuO_2, a second set of experiments were performed, but using a lower NO concentration (777 ppm), trying to simulate a NO concentration or real gas flows. Results showed that Li_2CuO_2 is able to consume NO in similar averages than those presented before. Nevertheless, the NO consumption times were extended as the Li_2CuO_2 particles surface saturation with $LiNO_3$ did not occur at least during 8 h of NO consumption. All these results proved that Li_2CuO_2 is able to perform the NSR process, and it would be considered as a possible candidate for NO sorption and selective catalytic reduction (NSR-SCR) as well.

CRediT authorship contribution statement

Ana Yañez-Aulestia: Data curation, Formal analysis, Investigation, Methodology, Writing - original draft, Writing - review & editing. **Heriberto Pfeiffer:** Conceptualization, Formal analysis, Funding acquisition, Investigation, Methodology, Project administration, Resources, Supervision, Visualization, Writing - original draft, Writing - review & editing.

Declaration of Competing Interest

The authors declare that they have no known competing financial interests or personal relationships that could have appeared to influence the work reported in this paper.

Acknowledgements

This work was financially supported by the project PAPIIT-UNAM IN-201419. The authors thank to A. Tejeda for technical assistance, while A. Yañez-Aulestia thanks the scholarship financial support to PNPC-CONACyT.

Appendix A. Supplementary data

Supplementary material related to this article can be found, in the online version, at doi:https://doi.org/10.1016/j.apcatb.2020.119119.

References

[1] E.M. Oziolor, N.M. Reid, S. Yair, K.M. Lee, S.G. VerPloeg, P.C. Bruns, J.R. Shaw, A. Whitehead, C.W. Matson, Science 364 (2019) 455–457.
[2] C. Wang, F. Yu, M. Zhu, X. Wang, J. Dan, J. Zhang, P. Cao, B. Dai, Chem. Eng. J. 346 (2018) 182–192.
[3] C. Liu, J.-W. Shi, C. Gao, C. Niu, Appl. Catal. A Gen. 522 (2016) 54–69.
[4] S. Deng, T. Meng, B. Xu, F. Gao, Y. Ding, L. Yu, Y. Fan, ACS Catal. 6 (2016) 5807–5815.
[5] K. Zhang, F. Yu, M. Zhu, J. Dan, X. Wang, J. Zhang, B. Dai, Catal. 8 (2018) 100–115.
[6] Z. Hong, Z. Wang, X. Li, Catal. Sci. Technol. 7 (2017) 3440–3452.
[7] Y. Wang, M. Makkee, Appl. Catal. B: Environ. 259 (2019) 117895.
[8] W.S. Epling, L.E. Campbell, A. Yezerets, N.W. Currier, J.E. Parks, Catal. Rev. Sci. Eng. 46 (2004) 163–245.
[9] Q.N. Tran, F. Martinovic, M. Ceretti, S. Esposito, B. Bonelli, W. Paulus, F. Di Renzo, F.A. Deorsola, S. Bensaid, R. Pirone, Appl. Catal. A Gen. 589 (2020) 117304.
[10] Z. Bai, B. Chen, Q. Zhao, C. Shi, M. Crocker, Appl. Catal. B: Environ. 249 (2019) 333–345.
[11] Y. Yu, J. Zhang, C. Chen, C. He, J. Miao, H. Li, J. Chen, J. Environ. Sci. 91 (2020) 237–245.
[12] Y. Yu, C. Chen, M. Ma, M. Douthwaite, C. He, J. Miao, J. Chen, C. Li, Chem. Eng. J. 361 (2019) 820–829.
[13] Z. Hong, Z. Wang, X. Li, Catal. Sci. Technol. 7 (2017) 3440–3452.
[14] W.S. Epling, L.E. Campbell, A. Yezerets, N.W. Currier, J.E. Parks, Catal. Rev. Sci. Eng. 46 (2004) 163–245.
[15] R. Burch, Catal. Rev. Sci. Eng. 46 (2004) 271–334.
[16] Y. Zhang, Y. Yu, W. Shan, Z. Lian, H. He, Catal. Today 339 (2020) 135–147.
[17] B.S. Kim, P.S. Kim, J. Bae, H. Jeong, C.H. Kim, H. Lee, Environ. Sci. Technol. 53 (2019) 2900–2907.
[18] S. Andonova, V. Marchionni, L. Lietti, L. Olsson, Mol. Catal. 436 (2017) 43–52.
[19] Z. Zhou, M.P. Harold, D. Luss, Appl. Catal. B: Environ. 255 (2019) 117742.
[20] Y. Cui, Q. Yan, C. Zhang, L. Qiu, Q. Wang, Catal. Commun. 101 (2017) 125–128.
[21] A.P. Soares-Dias, J. Bernardo, P. Felizardo, M.J. Neiva-Correia, Fuel Proc. Technol. 102 (2012) 146–155.
[22] J.A. Onrubia-Calvo, B. Pereda-Ayo, A. Bermejo-López, A. Caravaca, P. Vernoux, J.R. González-Velasco, Appl. Catal. B: Environ. 259 (2019) 118052.
[23] L. Lv, X. Wang, M. Shen, Q. Zhang, J. Wang, Chem. Eng. J. 222 (2013) 401–410.
[24] S.J. Castillo, M.S. Bensaid, F.A. Deorsola, N. Russo, D. Fino, Fuel 149 (2015) 78–84.
[25] V. Alcalde-Santiago, A. Davó-Quiñonero, I. Such-Basáñez, D. Lozano-Castelló, A. Bueno-López, Appl. Catal. B: Environ. 220 (2018) 524–532.
[26] Y. Bai, X. Bian, W. Wu, Appl. Surf. Sci. 463 (2019) 435–444.
[27] X. Zhou, X. Zhai, G. Ge, J. Dan, K. Pan, J. Tian, R. Sun, B. Dai, H. Pfeiffer, F. Yu, Chem. Eng. J. 388 (2020) 124270.
[28] Y. Yu, C. Chen, C. He, J. Miao, J. Chen, ChemCatChem 11 (2019) 979–984.
[29] C.A. Sierra-Pereira, E.A. Urquieta-Gonzalez, Fuel 118 (2014) 137–147.
[30] J. Xu, S. Renfrew, M.A. Marcus, M. Sun, B.D. McCloskey, W. Tong, J. Phys. Chem. C 121 (2017) 11100–11107.
[31] C.G. Han, C. Zhu, G. Saito, N. Sheng, T. Nomura, T. Akiyama, Electrochim. Acta 224 (2017) 71–79.
[32] C. Juarez-Yescas, M. Oliver-Tolentino, G. Ramos-Sánchez, M.A. Vera-Ramirez, J. Olmedo-González, A. Ochoa-Calle, A. Manzo-Robledo, F. González, I. González, ACS Appl. Energy Mater. 3 (2020) 2771–2780.
[33] A. Yañez-Aulestia, J.F. Gómez-García, J.A. Mendoza-Nieto, Y. Duan, H. Pfeiffer, Thermochim. Acta 660 (2018) 144–151.
[34] K. Oh-ishi, Y. Matsukura, T. Okumura, Y. Matsunaga, R. Kobayashi, J. Solid State Chem. 211 (2014) 162–169.
[35] H.A. Lara-García, B. Alcántar-Vázquez, Y. Duan, H. Pfeiffer, J. Phys. Chem. C 120 (2016) 3798–3806.
[36] F. Owens, J. Phys. C 313 (1999) 65–69.
[37] S. Kawamata, K. Okuda, K. Kindo, J. Magn. Magn. Mater. 272 (2004) 939–940.
[38] H.A. Lara-García, B. Alcántar-Vázquez, Y. Duan, H. Pfeiffer, RSC Adv. 5 (2015) 34157–34165.
[39] J.I. Langford, A.J.C. Wilson, J. Appl. Cryst. 11 (1978) 102–113.
[40] K.I. Hadjiivanov, Catal. Rev. Sci. Eng. 42 (2000) 71–144.
[41] M.L. Ruiz, I.D. Lick, M.I. Ponzi, E.R. Castellón, A. Jiménez-López, E.N. Ponzi, Thermochim. Acta 499 (2010) 21–26.
[42] S. Oohira, M. Kakihana, Y. Fujii, T. Nagumo, M. Okamoto, J. Nucl. Mater. 133–134 (1985) 201–204.
[43] P. Mars, D.W. Van-Krevelen, Chem. Eng. Sci. 3 (1954) 41–59.
[44] H.A. Lara-García, E. Vera, J.A. Mendoza-Nieto, J.F. Gómez-García, Y. Duan, H. Pfeiffer, Chem. Eng. J. 327 (2017) 783–791.
[45] S. Poulston, P.M. Parlett, P. Stone, M. Bowker, Surf. Interface Anal. 24 (1996) 811–820.
[46] H.A. Mosqueda, C. Vazquez, P. Bosch, H. Pfeiffer, Chem. Mater. 18 (2006) 2307–2310.